Journal of Power Sources 196 (2011) 3331–3341

Contents lists available at ScienceDirect

Journal of Power Sources

journal homepage: www.elsevier.com/locate/jpowsour

Characteristics of mechanochemically prepared host–guest hybrid nanocomposites of vanadium oxide and conducting polymers

Oleg Yu. Posudievsky[a,*], Olga A. Kozarenko[a], Vyacheslav S. Dyadyun[a], Scott W. Jorgensen[b], James A. Spearot[c,1], Vyacheslav G. Koshechko[a], Vitaly D. Pokhodenko[a]

[a] L.V. Pisarzhevsky Institute of Physical Chemistry of the National Academy of Sciences of Ukraine, 31 prospekt Nauki, Kiev 03028, Ukraine
[b] General Motors Research and Development Laboratories 480-106-160, 30500 Mound Road, Warren, MI 48090-9055, USA
[c] General Motors Research and Development Laboratories, USA

ARTICLE INFO

Article history:
Received 6 October 2010
Received in revised form
18 November 2010
Accepted 27 November 2010
Available online 4 December 2010

Keywords:
Host–guest
Nanocomposite
Cathode
Lithium ion battery
Mechanical milling
Conducting polymer

ABSTRACT

A set of two-component guest–host nanocomposites composed of conducting polymers and vanadium oxide are prepared *via* a single-step, solvent-free synthesis. The composition, structure, physical and electrochemical properties of these materials are studied. The nanocomposites have a guest–host structure, with the conducting polymer located in the interlayer space of the inorganic nanoparticles. The nanocomposites are capable of reversible cycling as the positive electrode in a lithium ion cell, and retain their capacity over one hundred full charge–discharge cycles. After cycling at a current of ~0.2 A g^{-1}, their capacity is restored when cycling at lower current, demonstrating the stability of their structure.

1. Introduction

Nanocomposite materials, with structure controlled at the nanoscale, have recently become a high priority field of scientific research and technical development [1]. The interest in these materials is high because very often they possess functional characteristics unattainable in macroscale analogues. As batteries are used in a wide range of devices in addition to the growing use in vehicles, the development of efficient nanostructured electrode materials and electrolytes for them is a world-wide research focus [2–5].

Lithium batteries attract special attention due to their exceptional functionality [5–7]. Transition metal oxides are the most studied cathode materials for lithium batteries at present [2,7–9]. That is dictated by their ability to form structures which allow insertion of lithium ions at high potential. But the specific capacity of the cobalt, nickel and manganese oxides most often used at present does not generally exceed ~150 mAh g^{-1}; this stimulates active research aimed at the development of more efficient, alternative, cathode materials.

Vanadium oxide, V_2O_5, possesses such important characteristics as high specific capacity, simplicity of synthesis and relatively low cost, so it has attracted close attention for a long time [8,10–16]. But along with high capacity crystalline V_2O_5 also has an essential drawback, bad cyclability [8]. More promising results are obtained for hydrated vanadium oxide xerogels – $V_2O_5{\cdot}nH_2O$ [15,17–19]. Xerogels, being nanostructured materials, possess important advantages due to their morphology: large electrochemically active external surface, small size particles and low density could promote high diffusion rate as well as small volume expansion during intercalation of lithium ions. The presence of water molecules between the layers increases the interlayer space and increases the capacity of $V_2O_5{\cdot}nH_2O$ in comparison to crystalline V_2O_5 [20,21]. Unfortunately, the stability of the structure towards intercalation/de-intercalation of lithium ions is insufficient and the initial high capacity of the xerogel quickly decreases upon cycling.

Conducting conjugated polymers (CCPs), which possess high inherent conductivity and are able to undergo practically fully reversible redox processes, present another perspective class of cathode material for lithium batteries [22,23]. The main drawbacks of CCP based cathodes are relatively low specific capacity and high self-discharge [22].

* Corresponding author. Tel.: +380 44 525 6672; fax: +380 44 525 6216.
E-mail addresses: posol@inphyschem-nas.kiev.ua (O.Yu. Posudievsky), scott.w.jorgensen@gm.com (S.W. Jorgensen).
[1] Retired.

0378-7753/$ – see front matter © 2010 Elsevier B.V. All rights reserved.
doi:10.1016/j.jpowsour.2010.11.153

Based on the facts presented above, it is natural to suppose that creation of hybrid nanocomposites from nanosized oxides and CCP, which might combine the attractive features of both materials – high capacity and ability to intercalate lithium ions of the oxides, and the high cyclability, conductivity, and other properties of the CCP – could be one of the promising routes for further progress in cathode materials. Several approaches are used for preparation of such hybrid nanocomposites. One of them is based on embedding inorganic nanoparticles in a CCP matrix [24–26]. Another method is insertion of CCP macromolecules inside interlayer galleries or channels of inorganic nanoparticles; this preparation of guest–host compounds can have new, attractive, functional properties [24,27–55]. Guest–host nanocomposites might be developed for layered inorganic matrixes such as vanadium and molybdenum oxides, in which CCP can stabilize the inorganic matrix during intercalation/deintercalation of lithium ions, increase the overall conductivity of the materials and the efficiency of its cycling while retaining the high discharge capacity of the inorganic component of the nanocomposite.

Synthesis of CCP/oxide based guest–host nanocomposites was first shown by Kanatzidis and co-workers [56–58]. Several methods for preparation of such nanocomposites are known now [59]: intercalative polymerization of monomers *in situ*; intercalation of monomers with subsequent polymerization under the effect of oxidant, application of heat, or microwave irradiation; direct intercalation of polymers inside the inorganic matrix; exfoliation of inorganic nanoparticles with their subsequent re-assembly with CCP incorporation. These methods for preparation of hybrid nanocomposites require, as a rule, use of liquid media and organic solvents since the monomers are often insoluble in water. Some preparation methods demand application of elevated temperature or hydrothermal conditions [59–62]. In addition, the materials prepared *via* these methods need thorough purification requiring the use of additional solvents.

Recently the possibility of solid state synthesis of guest–host hybrid nanocomposites as a result of mechanochemical reaction was shown [63–69]. Mechanochemical methods possess several advantages: they are ecologically clean, sufficiently cheap and simple, and have fairly high productivity [70,71].

Systematic research on guest–host hybrid nanocomposites prepared by the sol–gel method, which was carried out in recent years, has shown that such nanocomposites can possess excellent electrochemical characteristics [35,43,45,50], but the technological effectiveness of that method and the reproducibility of those characteristics were insufficient. In the present paper, guest–host hybrid nanocomposites based on CCP (polyaniline, polypyrrole, polythiophene) and vanadium oxide are prepared by mechanochemical methods, and their structure, spectral and electrochemical characteristics are studied with the aim of developing a method for preparation of nanocomposites with superior characteristics. Prolonged charge–discharge cycling is conducted, because in the literature it is uncommon to find data for hybrid nanocomposites tested over more than 20–30 cycles, complicating determination of their long term efficiency and their prospects for practical application.

2. Experimental

2.1. Reagents

Aniline (99%, Aldrich), pyrrole (98+%, Alfa Aesar), 2,2′-bithiophene (97%, Aldrich) and crystalline vanadium oxide V_2O_5 (99.99%, Aldrich) were used for preparation of hybrid nanocomposites. The aniline and pyrrole were distilled in vacuum before use.

The V_2O_5 xerogel was prepared by evaporation of an aqueous sol of V_2O_5, which was preliminarily synthesized by reaction of crystalline V_2O_5 with hydrogen peroxide [36], in a rotary evaporator followed by drying of the solid residue in vacuum at 100 °C.

Lithium metal (99.9%), anhydrous lithium perchlorate (battery grade, 99.99%), organic solvents, ethylene carbonate (99%), dimethyl carbonate (99+%) and poly(vinylidenefluoride-co-hexafluoropropylene) as a binder from Aldrich were used for fabrication of lithium battery prototypes; organic solvents were additionally purified by distillation directly before use.

2.2. Preparation of hybrid nanocomposites

The two-component hybrid composite samples of $(CCP)_{0.1}V_2O_5$ were prepared by mechanochemical treatment of the mixture of V_2O_5 xerogel and the proper monomer in an agate 80 mL grinding bowl containing thirty grinding balls with a diameter of 10 mm and nominal weight of 40 g. Samples were milled in a planetary Pulverisette 6 (Fritsch) for 9 h at 300 rpm. After mechanochemical treatment the product was separated by dry sieving.

Aliquots consisting of 2 g of $V_2O_5{\cdot}1.5H_2O$ xerogel and correspondingly 87 μL of aniline, 66 μL of pyrrole and 0.08 g of bithiophene were used for preparation of the composites based on polyaniline (PAn), polypyrrole (PPy) and polythiophene (PTh) respectively.

For characterization of the organic component of the composites by IR and NMR spectroscopies, it was isolated by filtration after dissolution of the inorganic component of the composites in 10% aqueous NaOH, thoroughly washed with water and ethanol and then it was dried in vacuum at 60 °C.

2.3. Characterization

Application of a C,H,N analyzer for determination of the composition of the prepared hybrid guest–host nanocomposite materials often led to incorrect results due to incomplete combustion of the polymer macromolecules located inside the interlayer galleries of the oxide matrix. Therefore the content of the inorganic component was confirmed spectrophotometrically using the ability of V^{5+} ions to form complexes with hydrogen peroxide in acid medium with a characteristic absorption at 405 nm [72]. The rest of the composite was considered as the organic part.

The powder X-ray diffraction of the prepared nanocomposites were conducted on a D8 ADVANCE (Bruker) diffractometer using filtered Cu Kα radiation in the range $2\theta = 1–70^\circ$ with an increment of 0.05°. Electron micrographs of the nanoparticles of the synthesized materials were obtained on a TEM125K (SELMI) microscope working at 100 kV. Amorphous carbon film which covered the copper grid was used as a carrier for the nanocomposite samples. SAED (selected area electron diffraction) patterns were also obtained on this facility.

Specific conductivity was measured using the standard four-probe method with an accuracy of 10%. The proper resistance of the contacts with tablets of the samples was achieved by gold plating the probe tips.

FTIR (Fourier transform infrared) spectra of the samples in KBr tablets were obtained using a SPECTRUM ONE (Perkin Elmer) spectrometer with a resolution of 2 cm^{-1}. ESR (electron spin resonance) spectra were obtained on E-9 spectrometer (Varian) using the signal of Mn^{2+} ions isomorphically substituted in the lattice of MgO as a standard. Solid-state CP MAS 13C NMR spectra were registered on Bruker 400 spectrometer with TMS as a standard.

Electrochemical studies were carried out in Swagelok cells, assembly of which was performed in a dry glove box filled with argon. A butt disk electrode served as the working electrode. The counter electrode, which was also used as the reference electrode,

was fabricated by press-fitting lithium foil to stainless steel mesh welded to the current collector. The cathode mass – composed of hybrid nanocomposite/conducting carbon additive/polymer binder in the ratio 75:15:10 – was formed under a pressure of 300 atm. The cathode tablet was pressed on stainless steel mesh and dried in vacuum at 80 °C during 12 h. The electrodes were separated by a polypropylene membrane impregnated with electrolyte. 1 M solution of $LiClO_4$ in an ethylene carbonate/dimethyl carbonate mixture (1:1, vol.%) served as the electrolyte. The content of water was not higher than 0.007%. Charge–discharge cycling was conducted using a computerized 32-channel facility in the range 2.0–4.0 V vs. Li/Li^+ at a constant current density in charge and discharge of 20 mA g^{-1}.

Impedance, galvanostatic quasiequilibrium discharge and cyclic voltammograms of the nanocomposites were taken using a μAUTOLAB III/FRA2 electrochemical analyzer (ECO CHEMIE) in a three-electrode cell, where the lithium plate was a counter electrode and lithium wire served as the reference electrode. The frequency dependence of impedance was measured in the range from 100 kHz to 0.75 mHz at different potentials after two full cycles of charge–discharge. The electrochemically active surface of the materials was estimated using the electrical double layer capacity measured using a smooth platinum electrode with known area. Modeling of the impedance spectra by equivalent circuits was performed using ZView2 software (Scribner).

Diffusion coefficients of lithium ions, D_{Li^+}, in the hybrid nanocomposites based on PAn and PPy were calculated by the equation [73,74]:

$$D_{Li^+} = \left[\frac{V_M}{\sqrt{2}F}\left(\frac{dE}{dx}\right)\frac{1}{AS}\right]^2,$$

where V_M is the molar volume of the studied material (cm^3 mole^{-1}), S is the active area of the electrode, (dE/dx) is the slope of the equilibrium potential on the quantity of the inserted lithium ions (x) at the fixed value of x during discharge or charge, A is the Warburg constant determined from impedance spectra, F is Faraday's constant. The value of V_M for the nanocomposites was determined based on the geometry of the composite assuming the volume expansion is confined to the interlayer spacing:

$$V_M = \frac{c}{c_0}V_{M_{V_2O_5}},$$

where c (c_0) is the interlayer distance in the nanocomposite (xerogel V_2O_5), $V_{M_{V_2O_5}} = 67.64$ cm^3 mole^{-1} or the molar volume of the xerogel V_2O_5. The value of dE/dx was measured using the curves of galvanostatic quasiequilibrium discharge at the current of 1 μA g^{-1}. For PTh based nanocomposites, the part of the spectra with 45° phase angle corresponding to the Warburgh impedance was absent on Nyquist diagrams; therefore the diffusion coefficient of lithium ions was calculated using the following formula [74]:

$$D_{Li^+} = \frac{l}{3R_W C_{int}},$$

where l is the characteristic length considered to be equal to the radius of the nanocomposite nanoparticles, R_W is the diffusion resistance, C_{int} is the charge capacity determined on the basis of the quasiequilibrium discharge curve.

3. Results and discussion

3.1. Structure of hybrid nanocomposites

Intercalative polymerization of such monomers as aniline, pyrrole and bithiophene as a result of mechanochemical treatment of the parent reagent mixture was confirmed by powder X-ray diffraction. From Fig. 1 one can see that there was an expansion

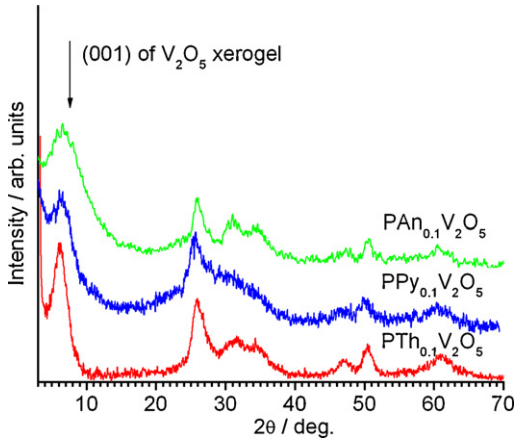

Fig. 1. X-ray diffractograms of the mechanochemically prepared nanocomposites.

of the interlayer space for $PAn_{0.1}V_2O_5$, $PPy_{0.1}V_2O_5$ and $PTh_{0.1}V_2O_5$ in comparison with the initial xerogel V_2O_5 as demonstrated by the shift of the (0 0 1) reflection in the lower angle region, whereas after mechanochemical treatment of the pure xerogel in analogous conditions the expansion of the interlayer space was not observed.

The observed changes in the XRD of the nanocomposites were due to insertion of CCP – PAn, PPy and PTh – inside the inorganic matrix consistent with formation of the guest–host nanocomposites [24,27–59]. The height of the interlayer galleries calculated on the basis of the XRD spectra was 0.48, 0.50 and 0.56 nm for $PAn_{0.1}V_2O_5$, $PPy_{0.1}V_2O_5$ and $PTh_{0.1}V_2O_5$ respectively. The stated differences in the values of the gallery heights correlate with the features of the inserted polymers. It has been shown earlier [75,76] that PAn and PPy form in a doped state in mechanochemical synthesis, while PTh forms in the weakly doped or even undoped state. The charge state of PAn and PPy macromolecules, caused by doping, could lead to relative decrease of the interlayer galleries' height in the nanocomposites with V_2O_5 due to electrostatic interaction in the guest–host system, which in the case of PTh would be considerably weaker or totally absent. Also the influence of the geometric factor – the size of the inserted polymer chains – must not be excluded [77,78].

It should be noted that $PTh_{0.1}V_2O_5$, in comparison with the other mechanochemically prepared nanocomposites, was characterized by the greatest ratio of the intensity of (0 0 1) peak height to its halfwidth (Fig. 1). It has been established [75] that the polymerization degree of PTh is rather low, about 10 in mechanochemical synthesis, which could promote greater ordering in separate nanoparticles of $PTh_{0.1}V_2O_5$ as compared with PAn and PPy based nanocomposites. The decrease of the polymerization degree probably led to the presence of PTh macromolecules inside only one particle of the hybrid nanocomposite, while in the case of PAn and PPy possessing a degree of higher polymerization, single macromolecules could extend to the inside of two or more particles, as well as outside of the inorganic matrix. This is consistent with the differences in the XRDs of the nanocomposites.

To trace the process of the mechanochemical initiation of the guest–host structure formation, on the example of $PTh_{0.1}V_2O_5$, we studied the effect of milling time of the initial xerogel V_2O_5/bithiophene mixture on the structure of the hybrid material (Fig. 2). As follows from the diffractograms presented in Fig. 2, partial insertion took place after 3 min, confirmed by the appearance of the nanocomposite peak (0 0 1) at about 6.5 and a decrease of the corresponding xerogel reflection intensity. After a 15 min treatment the reflection of the initial xerogel practically disappeared and there was only the nanocomposite (0 0 1) reflection. The decrease of the integral intensity of that reflection in comparison with anal-

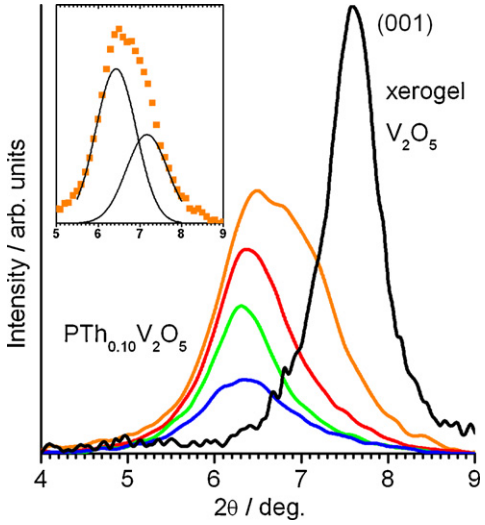

Fig. 2. Dependence of (0 0 1) reflex of $PTh_{0.1}V_2O_5$ nanocomposite on duration of the mechanochemical treatment: 1 – 3 min; 2 – 6 min; 3 – 9 min; 4 – 15 min. Inset: deconvolution of the reflex as a sum of the nanocomposite and xerogel signals.

ogous reflection of the xerogel results from the effect of electron density of the inserted macromolecules of CCP [79], decrease of the particle size, and disordering of $PTh_{0.10}V_2O_5$.

Micrographs and SAED patterns (Figs. 3–5) of the prepared hybrid nanocomposites showed that the synthesized materials consist of the aggregates of nanosized particles. In accord with Fig. 3a, the mechanochemically prepared nanocomposite $PPy_{0.1}V_2O_5$ was composed of polycrystalline particles with a size of 20–50 nm, consisting of separate crystallites which revealed themselves in the electronogram in the form of spot reflections superimposed on the ring diffraction pattern (Fig. 3b).

Unlike $PPy_{0.1}V_2O_5$, nanocomposite $PAn_{0.1}V_2O_5$, as seen in Fig. 4a, was composed of smaller nanoparticles forming textured structures which reveal themselves in the electronogram in the form of arcs (Fig. 4b). As the radial angle of these arcs is small, we suppose that the nanocomposite possessed high degree of texture due to an ordering effect of the polymer on the nanocomposite morphology as a result of the higher degree of polymerization of PAn as compared with PPy in the conditions of the mechanochemical synthesis [75]. Polymer chains of PAn could be situated in the adjacent nanocomposite particles, thereby ordering their relative position and demonstrating the texture of the material as a whole.

It follows from Figs. 3–5 that nanocomposite $PTh_{0.1}V_2O_5$, in comparison with the other two nanocomposites, was composed of smaller nanoparticles in the size range 5–10 nm (Fig. 5a). That was also confirmed by electronograms of $PTh_{0.1}V_2O_5$ characterized by increased width of the rings (Fig. 5b). That feature of the nanocomposite structure could be connected with the specificity of the mechanochemical synthesis of PTh which, as mentioned above, differed from PAn and PPy in lower degree of polymerization and a weakly doped state that obviously did not favor the aggregation of separate particles of the nanocomposite based thereon due to joint polymer chains as in the case of PAn and formation of the agglomerates of the nanosized particles as in the case of PPy.

It should be noted that in comparison with V_2O_5 xerogel and hybrid guest–host nanocomposites prepared by the sol–gel method, for which ribbon-like particles with the length of up to 1 μm are characteristic [20,80,81], as well as mechanochemically treated xerogel V_2O_5, which consisted of the particles with 200–400 nm characteristic size (Fig. 6), all three nanocomposites were formed of nanoparticles of considerably smaller size.

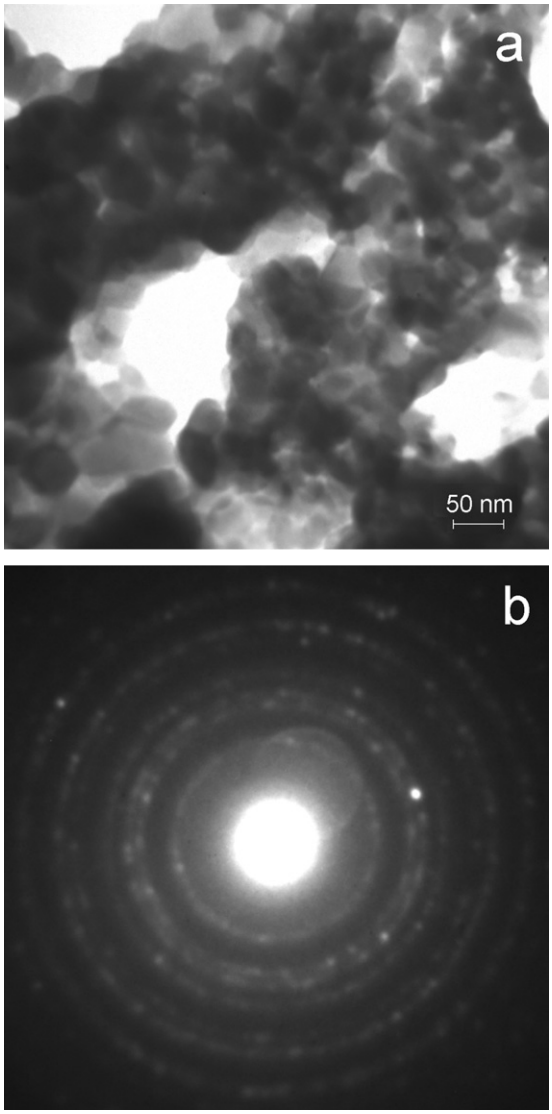

Fig. 3. TEM micrograph (a) and electronogram (b) of $PPy_{0.1}V_2O_5$ nanocomposite.

3.2. Conductivity of hybrid nanocomposites

Conductivities of the prepared nanocomposites are included in Table 1. The data show that conductivity of each hybrid material exceeded the conductivity of the initial xerogel. It was known [82] that the conductivity of the xerogel V_2O_5 depends on the average degree of oxidation, i.e. on the number of V^{4+} ions, because macroscopic electron transfer is realized by small polarons hopping between V^{5+} and V^{4+} centers. Taking that into account and also the fact that conductivity of the xerogel did not change as a result of the mechanochemical treatment (1.4×10^{-5} S cm^{-1}), the observed conductivity increases in the nanocomposites as compared with that of the xerogel is connected with the process of nanocomposite synthesis, specifically the oxidative polymerization

Table 1
Conductivity of the initial xerogel and the mechanochemically prepared nanocomposites.

Material	σ_{dc} (S cm^{-1})
Xerogel V_2O_5	1.0×10^{-5}
$PPy_{0.1}V_2O_5$	1.2×10^{-4}
$PAn_{0.1}V_2O_5$	9.6×10^{-5}
$PTh_{0.1}V_2O_5$	8.3×10^{-5}

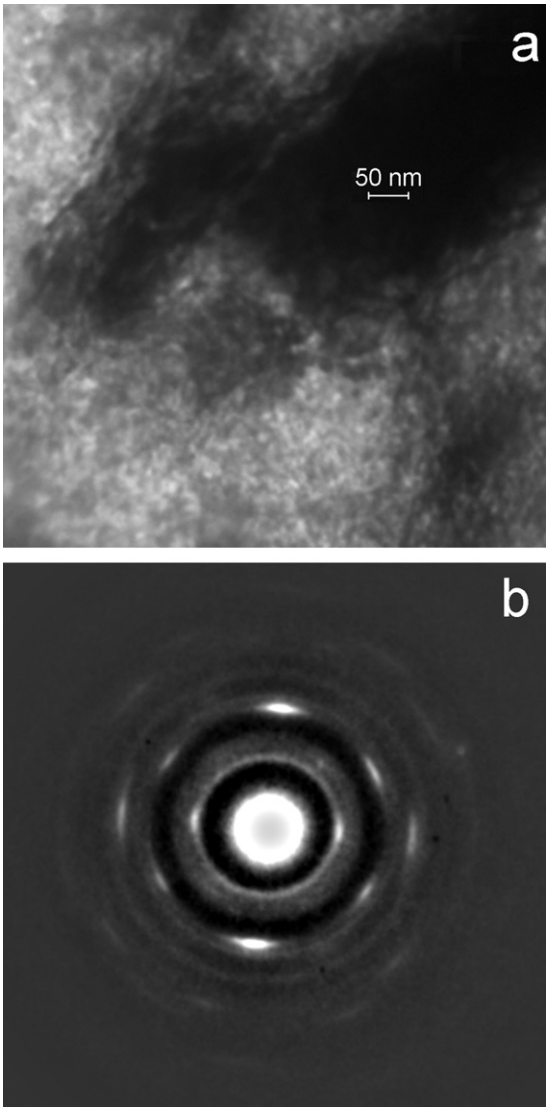

Fig. 4. TEM micrograph (a) and electronogram (b) of $PAn_{0.1}V_2O_5$ nanocomposite.

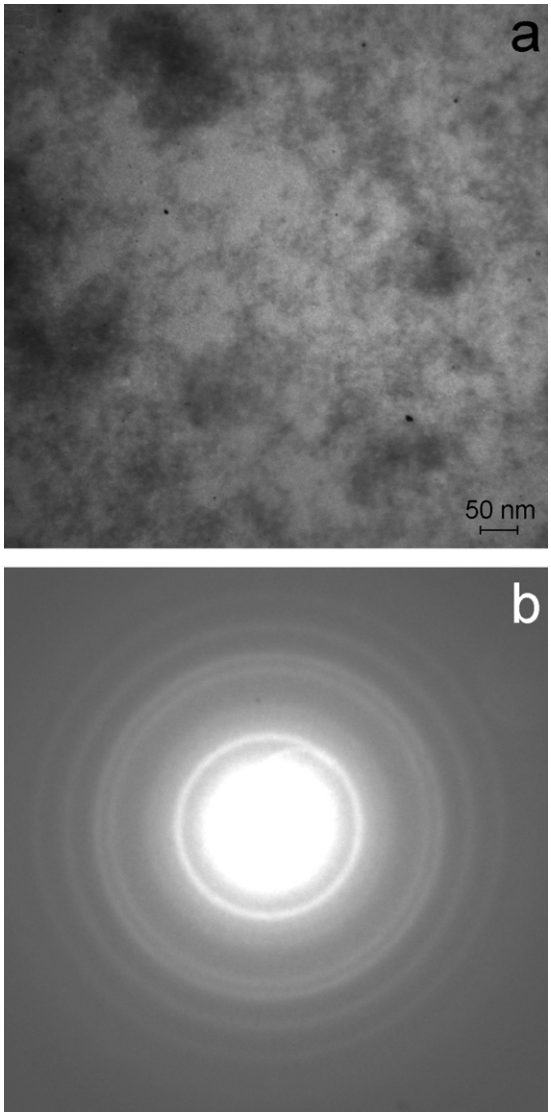

Fig. 5. TEM micrograph (a) and electronogram (b) of $PTh_{0.10}V_2O_5$ nanocomposite.

of the monomer by V_2O_5, during which partial reduction of V^{5+} to V^{4+} takes place increasing the content of V^{4+} centers in the inorganic component.

3.3. Spectral characteristics of hybrid nanocomposites

FTIR spectra of the prepared hybrid nanocomposites are presented in Fig. 7. The spectra contain bands characteristic of both inorganic (1000, 765, 527 cm^{-1}) [35,43,45] and CCP: PTh (1330, 1200, 1120 cm^{-1} and also a shoulder about 1030 cm^{-1}) [75], PPy (1560, 1480, 1300, 1200, 1050 cm^{-1}) [75] and PAn (1580, 1500, 1300, 1240, 1120 cm^{-1}) [76]. It should be mentioned here that the bands characteristic of PPy and PAn corresponded to their doped, conductive state: for $PPy_{0.1}V_2O_5$ nanocomposite, the presence of the bands about 1560 and 1480 cm^{-1} showed the existence of benzoid and quinoid heterostructures in the polymer chains, while for the $PAn_{0.1}V_2O_5$ nanocomposite, the conducting state of the polymer was established by the presence of the band about 1120 cm^{-1}. The FTIR spectra confirmed a redox mechanism of the mechanochemical intercalative polymerization, during which the inorganic host, V_2O_5, possessing sufficiently high oxidative potential, initiated polymerization of the correspondent monomers as well as the doping of the guest polymer.

FTIR (Fig. A12a, Appendix) and solid-state CP MAS 13C NMR (Fig. A12b, Appendix) spectra of the isolated organic components of the studied nanocomposites showed that polymerization degree of the corresponding polymers is in accord

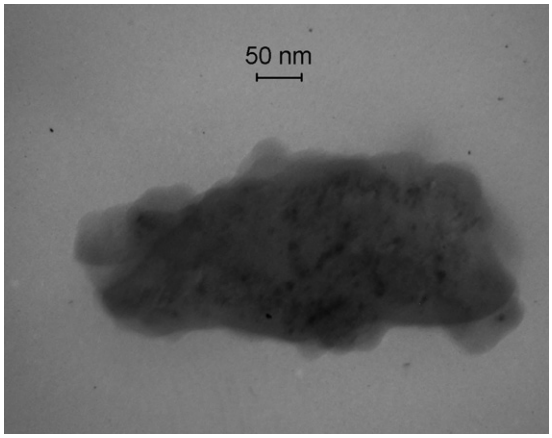

Fig. 6. TEM micrograph of mechanochemically treated V_2O_5 xerogel.

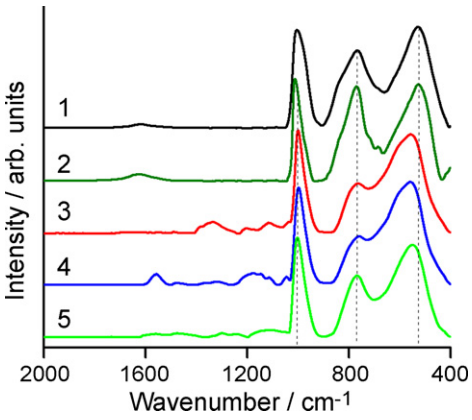

Fig. 7. FTIR spectra of V_2O_5 xerogel (1), mechanochemically treated V_2O_5 xerogel (2) and hybrid nanocomposites $PTh_{0.1}V_2O_5$ (3), $PPy_{0.1}V_2O_5$ (4) and $PAn_{0.1}V_2O_5$ (5).

with the data obtained earlier for solvent-free preparation of CCP [75,76].

Comparison of FTIR spectra of $PTh_{0.1}V_2O_5$, $PPy_{0.1}V_2O_5$ and $PAn_{0.1}V_2O_5$ nanocomposites with the spectra of xerogel showed the presence of a blue shift of ~30 cm^{-1} in $\nu_{s,V-O-V}$ band of the inorganic matrix about 530 cm^{-1} (Fig. 7). Such a shift was absent in the spectra of both mechanochemically treated xerogel (Fig. 7) and analogous nanocomposites prepared by the sol–gel method [28,34,36,37,43,45,73]. In our opinion, the observed shift of $\nu_{s,V-O-V}$ was the consequence of disordering in the V_2O_5 lattice induced by the simultaneous effect of both mechanical forces and partial reduction of V_2O_5 (in comparison with the xerogel) during preparation of the nanocomposites.

ESR spectra of the hybrid nanocomposites are presented in Fig. 8. There is obvious hyperfine structure in the spectrum of the initial xerogel V_2O_5 indicating the existence of V^{4+} ions. In contrast to that, in the spectra of the nanocomposites, there was only one intense singlet with $g = 1.972 \pm 0.002$ and there was no signal from the paramagnetic centers of CCP which are cation-radicals in the doped state. The absence of the hyperfine interaction due to V^{4+} ions was connected with an increasing degree of reduction in the inorganic matrix during mechanochemical polymerization and formation of paramagnetic V^{4+} ions [43] while the absence of the signal from the organic radicals was due to quick antiferromagnetic exchange of the unpaired electrons between V^{4+} and the polymer

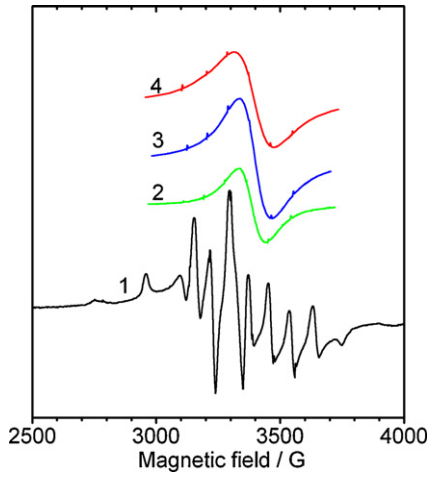

Fig. 8. ESR spectra of V_2O_5 xerogel (1), $PAn_{0.1}V_2O_5$ (2), $PPy_{0.1}V_2O_5$ (3) and $PTh_{0.1}V_2O_5$ (4) (the sextet signal of the standard is seen on the spectra, which are vertically shifted for convenience).

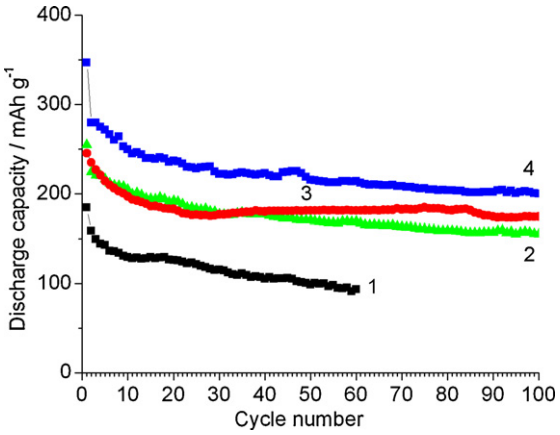

Fig. 9. Cycling of V_2O_5 xerogel (1) and mechanochemically prepared nanocomposites at specific current $I_0 = 20$ mA g^{-1}: $PAn_{0.1}V_2O_5$ (2), $PTh_{0.1}V_2O_5$ (3) and $PPy_{0.1}V_2O_5$ (4).

chains [56,57], one more piece of evidence in favor of the formation of the guest–host hybrid nanocomposites.

3.4. Charge–discharge cycling of hybrid nanocomposites

Results of prolonged charge–discharge cycling of the guest–host hybrid nanocomposites $PAn_{0.1}V_2O_5$, $PTh_{0.1}V_2O_5$ and $PPy_{0.1}V_2O_5$ as well as V_2O_5 xerogel are presented in Fig. 9. This figure indicates that the specific capacity of the hybrid nanocomposites considerably exceeds analogous characteristics of both the initial xerogel and the inserted CCP (120, 80 and 40 mAh g^{-1} for PAn, PPy and PTh respectively [22]). Among the synthesized nanocomposites, $PPy_{0.1}V_2O_5$ possessed the greatest capacity. Along with high specific capacity the mechanochemically prepared nanocomposites were capable to prolonged cycling during which the capacity stabilized and practically did not change during last 70 charge–discharge cycles.

We attribute this degree of stability to the stabilizing effect of CCP on the inorganic matrix and improved access to Li^+ intercalation center ions due to expansion of the interlayer galleries in the xerogel. To the best of our knowledge, the specific capacity and cyclability of the mechanochemically prepared hybrid nanocomposites exceed those of analogous materials prepared by other methods [28,32–34,36,37,40–43,45,73].

When creating new cathode materials for lithium batteries, great attention is devoted to their capability for cycling at high charge–discharge currents. In this connection, we studied cycling of the three nanocomposites at currents equal to $5I_0$ and $10I_0$ (where I_0 is the C rate). Results are shown in Fig. 10. It follows from that data that the specific capacity of the nanocomposites decreased with increasing rate of discharge but stabilized at some value, and for high current tests up to $I_0 = 20$ mA g^{-1} upon returning to the initial discharge current the capacity returned to its initial value. The capacity retention of the three nanocomposites at high current fell in the order $PPy_{0.1}V_2O_5 > PTh_{0.1}V_2O_5 > PAn_{0.1}V_2O_5$, thus the nanocomposite with the highest capacity possessing the best stability towards increased discharge currents. It is important to note that all nanocomposites regained their capacity when the discharge current returned to I_0, which indicates their stability to degradation. It is also interesting that the data show $PPy_{0.1}V_2O_5$ was composed of the largest nanoparticles, according to the TEM data (Figs. 3–5). Taking that into account, it can be concluded that including the effect of the polymer guest, the size of the nanocomposite particles was not determining in the charge–discharge cycling in the size range produced in these experiments.

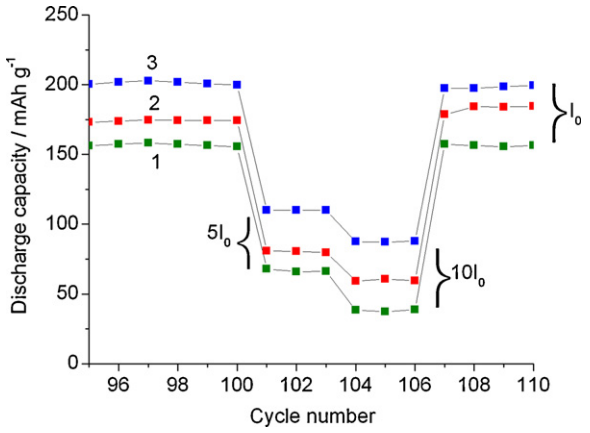

Fig. 10. Cycling of mechanochemically prepared nanocomposites at specific currents I_0 (20 mA g^{-1}), $5I_0$ and $10I_0$: $PAn_{0.1}V_2O_5$ (1), $PTh_{0.1}V_2O_5$ (2) and $PPy_{0.1}V_2O_5$ (3).

To elucidate this effect in detail we conducted comparative studies of the prepared hybrid nanocomposites by cyclic voltammetry. Cyclic voltammograms (CVA) of the considered materials are presented in Fig. 11, from which it follows that two main reversible electrochemical processes took place in the xerogel as well as in the hybrid nanocomposites, revealed in the form of wide peaks about 2.9 and 2.4 V. According to Imamura and Miyayama [83], the noted peaks corresponded to interaction of Li^+ ions with *a*- and *b*-centers, the first being located in the center of the square formed by oxygen atoms in the base of VO_5 pyramid and the second – near the vanadyl oxygen. The redox activity of the polymers inserted in the V_2O_5 was not manifested explicitly due to their small proportion of the nanocomposite's composition.

To clarify the features of intercalation of Li^+ ions inside the structure of the nanocomposites we measured quasiequilibrium discharge curves and differential capacity plots calculated on their basis, which are presented in Fig. 12 for initial xerogel, mechanochemically treated xerogel and $PAn_{0.1}V_2O_5$, $PPy_{0.1}V_2O_5$ and $PTh_{0.1}V_2O_5$ nanocomposites. The character of the obtained quasiequilibrium discharge curves corresponds to the form of the CVA: the potential monotonically decreased and was formed of smoothed, weakly expressed plateaus. Such plateaus could be due to the presence of a variety of intercalation centers for Li^+ ions with different energy, a manifestation of the rather disordered state of the structure of the materials [84]. Thus it is more convenient to consider the intercalation process using differential capacity

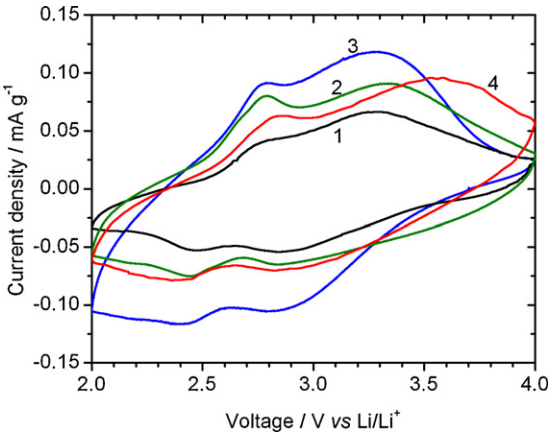

Fig. 11. Cyclic voltammograms (CVA) of the initial xerogel (1) and $PAn_{0.1}V_2O_5$ (2), $PPy_{0.1}V_2O_5$ (3) and $PTh_{0.1}V_2O_5$ (4) nanocomposites. CVA were registered in 1 M solution of $LiClO_4$ in EC/DMC (1:1, vol.%) at potential scan rate 0.1 mV s^{-1}.

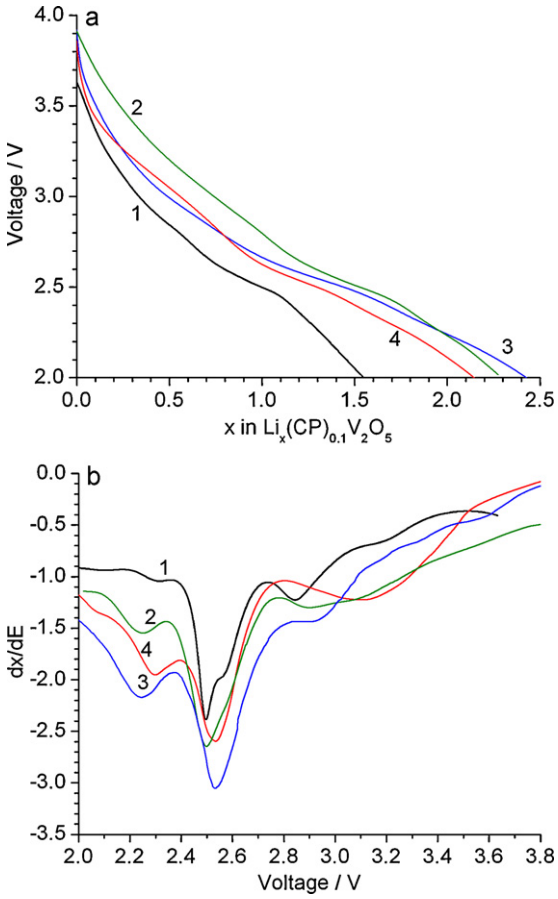

Fig. 12. Quasiequilibrium discharge (a) and differential capacity (b) curves of the initial xerogel (1) and $PAn_{0.1}V_2O_5$ (2), $PPy_{0.1}V_2O_5$ (3) and $PTh_{0.1}V_2O_5$ (4) nanocomposites. Chronoamperograms were registered in 1 M solution of $LiClO_4$ in EC/DMC (1:1, vol.%) at specific current 1 μA g^{-1}.

curves: as can be seen from Fig. 12b, two main peaks about 2.85 and 2.50 V, which are identical to those on CVA of the xerogel (Fig. 11), were clearly defined on the differential capacity curves of the xerogel.

Differential capacity curves of the nanocomposites were significantly different from those of the xerogel V_2O_5. For instance, the process corresponding to intercalation of Li^+ ions in *b*-centers of the hybrid nanocomposites proceeded at nearly the same potential as in the xerogel. That observation agrees with the invariant position of the FTIR band at about 1000 cm^{-1} determined by vibration of the V=O bonds in the xerogel and in the hybrid nanocomposites (Fig. 7). Meanwhile, the potential corresponding to intercalation of Li^+ ions in *a*-centers shifted up by 60, 80 and 250 mV respectively for $PAn_{0.1}V_2O_5$, $PPy_{0.1}V_2O_5$ and $PTh_{0.1}V_2O_5$. The observed shifts correspond to easier intercalation of Li^+ ions, their values ordering similarly to the changing heights of the interlayer galleries in the nanocomposites (correspondingly 0.48, 0.50 and 0.56 nm).

It should be noted that in all three nanocomposites there was a process that proceeds at a potential of 2.25–2.30 V (Fig. 12b) and the nature of which is not so evident at present. The presence of that process was confirmed by CVA (Fig. 11) where there was a bend at a potential of 2.3 V for the prepared nanocomposites. The potential suggests that there could be an amount of crystalline V_2O_5 in the nanocomposites where a phase transition takes place at 2.2 V during intercalation of Li^+ ions [8]. The appearance of the crystalline V_2O_5 phase is connected with the synthesis conditions of the nanocomposites. During mechanochemical treatment a rather high amount of local heat was generated as a result of the numerous

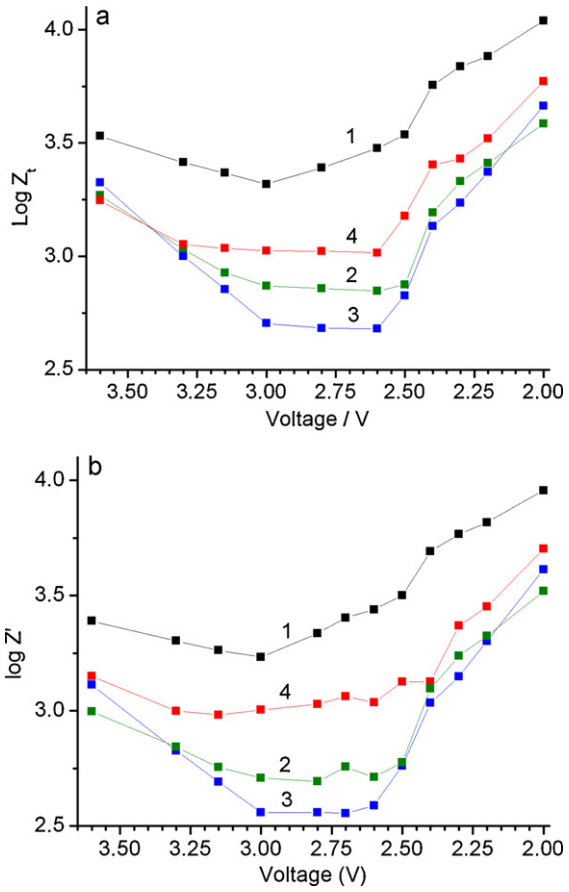

Fig. 13. Dependence of the total impedance Z_t (a) and its real component Z' (b) on potential (f = 0.75 mHz) for the initial xerogel (1) and $PAn_{0.1}V_2O_5$ (2), $PPy_{0.1}V_2O_5$ (3) and $PTh_{0.1}V_2O_5$ (4) nanocomposites.

collisions between the grinding balls and the grinding bowl walls. That heat could induce formation of crystalline V_2O_5 after removal of the remaining water from the interlayer space of the xerogel.

On the other hand, as it is known [8], the irreversible phase transformations in crystalline V_2O_5 at 2.2 V is accompanied by a decrease of the specific capacity in cycling up to 2.0 V. This decrease in capacity is associated [8] with a loss of material integrity due to a sharp increase of the crystal lattice parameter a. However, as shown above for the three hybrid nanocomposites, there was no significant decrease in the specific capacity even at prolonged cycling. That fact provides support for the presence of CCP macromolecules inside the interlayer space of the prepared nanocomposites together with some changes in the structure of the inorganic matrix (expansion of the interlayer space, shift of $\nu_{s,V-O-V}$ band, redistribution of intensity between the $\nu_{as,V-O-V}$ and $\nu_{s,V-O-V}$ bands) prevented major changes of the a parameter and, as a consequence, improved the cyclability of the prepared hybrid nanomaterials.

3.5. Impedance of hybrid nanocomposites

Impedance spectroscopy, which reveals electrochemical processes proceeding at different characteristic rates, was used for more detailed study of the electrochemical behavior of the synthesized nanomaterials.

Dependence of the total impedance (Z_t) at 0.75 mHz, on the potential (V) of the hybrid nanocomposites and V_2O_5 xerogel, is presented in Fig. 13a. The use of a low value of frequency allowed us to assume the changes in Z_t were determined by the real component of the impedance (Z'), because at frequency tending to zero the total impedance Z_t is mainly determined by active resistance as seen in Fig. 13b. In Fig. 13a it is clear that the value of Z_t of the xerogel decreased significantly at the beginning of discharge and reached its minimum at a potential of 3.0 V, corresponding to the potential of Li^+ ions intercalation in the a-centers. Thereafter the value increased, until at a potential of 2.5 V – the potential of Li^+ ions intercalation in b-centers – it rose abruptly. Such a dependence of Z_t on the potential correlated with the data from Huguenin and Torresi [85], where the change of the xerogel resistance was measured *in situ* during discharge.

Dependence of Z_t as well as Z' on potential for mechanochemically prepared nanocomposites differed appreciably from that of xerogel V_2O_5 (Fig. 13). The difference in the value of Z_t, which was up to one order of magnitude, was obvious. The lowest value of Z_t was observed for $PPy_{0.1}V_2O_5$ while the greatest was seen with $PTh_{0.1}V_2O_5$, which is consistent with the values of conductivity σ_{dc} of the nanocomposites presented in Table 1. Additionally, for each nanocomposite there was an interval of potential in which the value of Z_t changed insignificantly and was nearly constant. The beginning and end of the interval corresponded to the potential for Li^+ ions intercalation in the a-centers and b-centers respectively (Fig. 12). This feature of Z_t for the nanocomposites can be linked with the presence of the polymer macromolecules inside the interlayer space of the inorganic matrix, because that is the principal difference between the structures of the nanocomposites and xerogel. One of the causes of the observed dependence Z_t (V) could be the influence of the inserted polymers on ionic conductivity of the nanocomposites; this is an area that could benefit from additional study.

Nyquist plots of the xerogel V_2O_5 and $PPy_{0.1}V_2O_5$ nanocomposite, which had the best specific capacity (Fig. 8), are presented in Fig. 14. At a potential of 3.6 V the impedance spectrum of the xerogel consisted of a high frequency semicircle, a slant line with phase angle of 45° at middle frequencies, and low frequency response of a slant line with a phase angle greater than 45°. The form of the impedance spectrum of the $PPy_{0.1}V_2O_5$ nanocomposite differed substantially from that of the xerogel as a low frequency semicircle began to appear. That low frequency response in consistency with results of the analysis performed in the Appendix using equivalent circuits from Ref. [86], was interpreted as being due to the presence of the CCP in the nanocomposite in the doped, conducting state.

Another significant difference in the impedance spectra of the initial xerogel V_2O_5 and the $PPy_{0.1}V_2O_5$ nanocomposite is the change of the high frequency semicircle at different potentials. Changing the potential from 3.6 V to 2.8 V causes the high frequency semicircle corresponding to charge transfer through the electrolyte/cathode interface to broaden appreciably in case of the xerogel (Fig. 14). This broadening is due to a considerable increase in the charge transfer resistance R_{ct}, whereas for $PPy_{0.1}V_2O_5$ the value of R_{ct} changed insignificantly (Table 2). Also, there was no obvious low frequency semicircle in the spectra of the nanocomposite below 2.8 V that could be connected with reduction (un-doping) of the inserted polymer guest (see Appendix).

It is important that the values of characteristic frequencies of key electrochemical processes such as charge transfer through the electrolyte/cathode interface, and solid state diffusion of lithium ions were higher in the nanocomposite than in the xerogel. In the case of the nanocomposite, the f_{ct} frequency, which is connected with interface charge transfer, was significantly higher (Fig. 14) and indicates more efficient intercalation of Li^+ ions. No less remarkable is the frequency f_d, being the characteristic of the rate of the solid state diffusion of Li^+ ions, which appeared to be considerably higher in the nanocomposite than in the xerogel. Its value in the nanocomposite may be determined up to potential of 2.6 V, while in the xerogel only up to 3.0 V. Quicker diffusion of Li^+ ions in the hybrid nanocomposite is obviously the effect of the

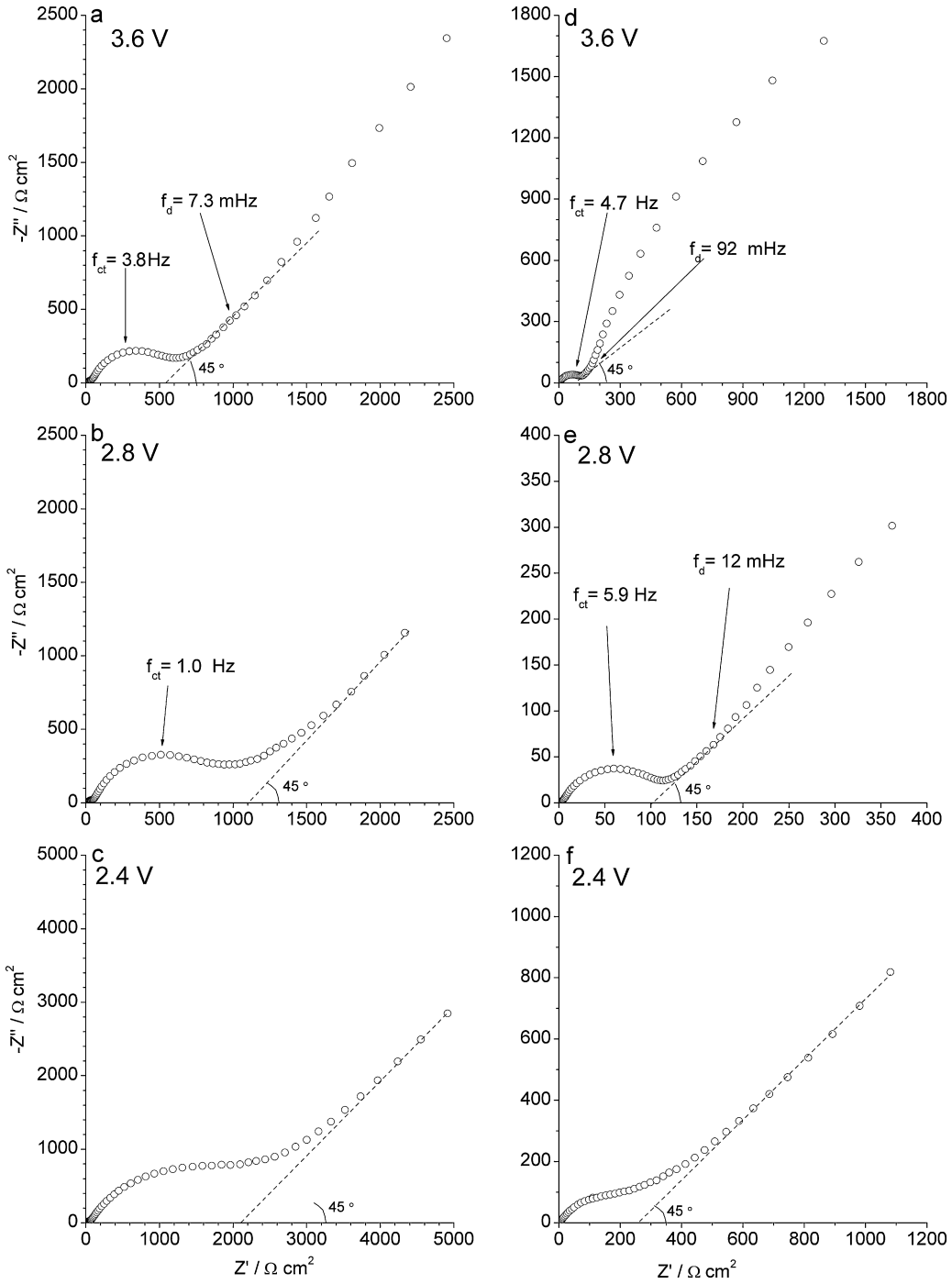

Fig. 14. Nyquist plots of the initial xerogel (a, b, c) and $PPy_{0.1}V_2O_5$ nanocomposite (d, e, f) at potentials 3.6, 2.8 and 2.4 V respectively.

Table 2
Diffusion coefficient D_{Li^+} and charge transfer resistance R_{ct} calculated based on the impedance spectra of the initial xerogel and the mechanochemically prepared nanocomposites.

V (V)	Xerogel V_2O_5		$PPy_{0.1}V_2O_5$		$PAn_{0.1}V_2O_5$		$PTh_{0.1}V_2O_5$	
	D_{Li^+} ($cm^2\ s^{-1}$)	R_{ct} ($\Omega\ cm^2$)	D_{Li^+} ($cm^2\ s^{-1}$)	R_{ct} ($\Omega\ cm^2$)	D_{Li^+} ($cm^2\ s^{-1}$)	R_{ct} ($\Omega\ cm^2$)	D_{Li^+} ($cm^2\ s^{-1}$)	R_{ct} ($\Omega\ cm^2$)
3.6	1.2E−10	540	1.1E−9	114	7.0E−10	77	2.2E−9	270
3.3	9.2E−11	486	7.7E−10	88	3.5E−10	73	4.4E−10	277
3.15	6.3E−11	471	6.4E−10	91	3.4E−10	71	2.5E−10	280
3.0	6.2E−11	540	5.8E−10	92	3.3E−10	72	1.7E−10	293
2.8	2.9E−11	946	5.1E−10	103	3.2E−10	80	1.4E−10	300
2.6	–	1.7E3	1.2E−10	111	8.3E−11	104	–	346
2.5	–	2.0E3	5.2E−11	198	4.1E−11	267	–	344
2.4	–	2.6E3	2.2E−11	319	3.3E−11	381	–	356

polymer inserted inside the interlayer galleries of the inorganic host.

It should be noted that, in comparison with the V_2O_5 xerogel, higher values of the diffusion coefficient D_{Li^+}, and lower values of the charge transfer resistance R_{ct} were also observed at lower potentials for mechanochemically prepared hybrid nanocomposites (Table 2). The impedance spectroscopy data and modeled results using equivalent electric circuits are presented in the Appendix. Practically complete absence of a passivation layer on the surface of the nanocomposite cathodes due to their interaction with the electrolyte should be particularly noted. This interpretation follows from the equivalent circuits A2 to A4, as well as the electrochemical activity of PAn and PPy inserted inside xerogel, which appeared in A2 and A3 as the presence of the element R_b, and the absence of that element in the equivalent circuit of the PTh based nanocomposite.

4. Conclusions

We have developed a method for mechanochemical preparation of two-component guest–host nanocomposites composed of conducting polymers (polyaniline, polypyrrole and polythiophene) and vanadium oxide. The method allows preparation *via* a single-step, solvent-free synthesis without need for post-synthesis purification.

The composition, structure, spectral, magnetic-resonance, electrical and electrochemical properties of these materials were studied by means of mutually complementary methods. It was established that the nanocomposites had a guest–host structure, with the conducting polymer located in the interlayer space of the inorganic nanoparticles. The nanoparticles were considerably smaller than those of the initial xerogel, a mechanochemically treated xerogel, as well as analogous nanocomposites prepared by the sol–gel method.

The nanocomposites showed that they were capable of reversible cycling, and possessed a discharge capacity ~200–250 mAh g^{-1} over at least one hundred cycles of full charge–discharge as the cathode of a lithium ion cell. The polypyrrole based nanocomposite had the greatest capacity. After cycling at a current of ~0.2 A g^{-1}, their capacity was restored when cycling at lower current, demonstrating the stability of their structure.

It was established that intercalation of lithium ions in the nanocomposites was more efficient than in the initial xerogel V_2O_5 due to higher diffusion rate of Li^+ ions and the absence of a detectible passivation film on the surface of the nanoparticles. We believe the higher discharge capacity, stability in prolonged charge–discharge cycling, and improved diffusion of lithium ions in the nanocomposites, are the consequences of pillaring by the conducting polymer macromolecules in the layers of the inorganic matrix.

Acknowledgments

We wish to thank Dr. Abbas Nazri who confirmed the electrochemical results. The work was supported by a contract from GM.

Appendix A. Supplementary data

Supplementary data associated with this article can be found, in the online version, at doi:10.1016/j.jpowsour.2010.11.153.

References

[1] H.S. Nalwa (Ed.), Handbook of Nanostructured Materials and Nanotechnology, Academic Press, San Diego, 2000.
[2] J. Schoonman, Solid State Ionics 157 (2003) 319–326.
[3] A.S. Aricò, P. Bruce, B. Scrosati, J.-M. Tarascon, W. van Schalkwijk, Nat. Mater. 4 (2005) 366–377.
[4] P. Balaya, A.J. Bhattacharyya, J. Jamnik, Yu.F. Zhukovskii, E.A. Kotomin, J. Maier, J. Power Sources 159 (2006) 171–178.
[5] M. Winter, R.J. Brodd, Chem. Rev. 104 (2004) 4245–4270.
[6] A. Ritchie, W. Howard, J. Power Sources 162 (2006) 809–812.
[7] B. Scrosati, J. Garche, J. Power Sources 195 (2010) 2419–2430.
[8] M.S. Whittingham, Chem. Rev. 104 (2004) 4271–4302.
[9] L.J. Fu, H. Liu, C. Li, Y.P. Wu, E. Rahm, R. Holze, H.Q. Wu, Prog. Mater. Sci. 50 (2005) 881–928.
[10] C. Delmas, H. Cognac-Auradou, J.M. Cocciantelli, M. Ménétrier, J.P. Doumerc, Solid State Ionics 69 (1994) 257–264.
[11] Y. Wang, K. Takahashi, K. Lee, G. Cao, Adv. Funct. Mater. 16 (2006) 1133–1144.
[12] S.H. Ng, S.Y. Chew, J. Wang, D. Wexler, Y. Tournayre, K. Konstantinov, H.K. Liu, J. Power Sources 174 (2007) 1032–1035.
[13] P. Ragupathy, S. Shivakumara, H.N. Vasan, N. Munichandraiah, J. Phys. Chem. C 112 (2008) 16700–16707.
[14] Y.-S. Hu, X. Liu, J.-O. Müller, R. Schlögl, J. Maier, D.S. Su, Angew. Chem. Int. Ed. 48 (2009) 210–214.
[15] D. Liu, Y. Liu, B.B. Garcia, Q. Zhang, A. Pan, Y.-H. Jeong, G. Cao, J. Mater. Chem. 19 (2009) 8789–8795.
[16] J.-K. Lee, G.-P. Kim, I.K. Song, S.-H. Baeck, Electrochem. Commun. 11 (2009) 1571–1574.
[17] S. Passerini, W.H. Smyrl, M. Berrettoni, R. Tosici, M. Rosolen, R. Marassi, F. Decker, Solid State Ionics 90 (1996) 5–14.
[18] S. Mège, Y. Levieux, F. Ansart, J.M. Savariault, A. Rousset, J. Appl. Electrochem. 30 (2000) 657–664.
[19] C.C. Torardi, C.R. Miao, M.E. Lewittes, Z. Li, J. Solid State Chem. 163 (2002) 93–99.
[20] J. Livage, Chem. Mater. 3 (1991) 578–593.
[21] G.T. Chandrappa, N. Steunou, J. Livage, Nature 416 (2002) 702.
[22] P. Novák, K. Müller, K.S.V. Santhanam, O. Haas, Chem. Rev. 97 (1997) 207–282.
[23] G. Inzelt, Conducting Polymers, Springer, Berlin, 2008.
[24] P. Gómez-Romero, C. Sanchez (Eds.), Functional Hybrid Materials, Wiley-VCH, Weinheim, 2003.
[25] Y. Mosqueda, E. Pérez-Cappe, G. Rodríguez, J.A. Varela, E. Souza, Phys. Stat. Sol. (C) 2 (2005) 3774–3777.
[26] L.-J. Her, J.-L. Hong, C.-C. Chang, J. Power Sources 157 (2006) 457–463.
[27] F. Leroux, B.E. Koene, L.F. Nazar, J. Electrochem. Soc. 143 (1996) L181–L183.
[28] F. Leroux, G.R. Goward, W.P. Power, L.F. Nazar, J. Electrochem. Soc. 144 (1997) 3886–3895.
[29] G.R. Goward, F. Leroux, L.F. Nazar, Electrochim. Acta 43 (1998) 1307–1313.
[30] H.P. Oliveira, C.F.O. Graeff, C.L.P.S. Zanta, A.C. Galina, P.J. Gonçalves, J. Mater. Chem. 10 (2000) 371–375.
[31] Y. Xiao, K.A. Hu, Q.C. Yu, R.J. Wu, J. Appl. Polym. Sci. 80 (2001) 2162–2166.
[32] F. Huguenin, R.M. Torresi, D.A. Buttry, J.E. Rereira da Silva, S.I. Córdoba de Torresi, Electrochim. Acta 46 (2001) 3555–3562.
[33] F. Huguenin, M.J. Giz, E.A. Ticianelli, R.M. Torresi, J. Power Sources 103 (2001) 113–119.
[34] A.V. Murugan, B.B. Kale, C.-W. Kwon, G. Campet, K. Vijayamohanan, J. Mater. Chem. 10 (2001) 2470–2475.
[35] O.Yu. Posudievsky, S.A. Biskulova, V.D. Pokhodenko, J. Mater. Chem. 12 (2002) 1446–1449.
[36] N.-G. Park, K.S. Ryu, Y.J. Park, M.G. Kang, D.-K. Kim, S.-G. Kang, K.M. Kim, S.-H. Chang, J. Power Sources 103 (2002) 273–279.
[37] C.-W. Kwon, A.V. Murugan, G. Campet, J. Portier, B.B. Kale, K. Vijayamohanan, J.-H. Choy, Electrochem. Commun. 4 (2002) 384–387.
[38] W. Chen, Q. Xu, Y.S. Hu, L.Q. Mai, Q.Y. Zhu, J. Mater. Chem. 12 (2002) 1926–1929.
[39] Y. Matsuo, S. Higashika, K. Kimura, Y. Miyamoto, T. Fukutsuka, Y. Sugie, J. Mater. Chem. 12 (2002) 1592–1596.
[40] F. Huguenin, E.M. Girotto, R.M. Torresi, D.A. Buttry, J. Electroanal. Chem. 536 (2002) 37–45.
[41] P. Gomez-Romero, M. Chojak, K. Cuentas-Gallegos, J.A. Asensio, P.J. Kulesza, N. Casan-Pastor, M. Lira-Cantu, Electrochem. Commun. 5 (2003) 149–153.
[42] F. Huguenin, E.M. Girotto, G. Ruggeri, R.M. Torresi, J. Power Sources 114 (2003) 133–136.
[43] O.Yu. Posudievsky, S.A. Biskulova, V.D. Pokhodenko, J. Mater. Chem. 14 (2004) 1419–1423.
[44] E.C. Zampronio, H.P. Oliveira, Mater. Res. Bull. 39 (2004) 1525–1538.
[45] O.Yu. Posudievsky, S.A. Biskulova, V.D. Pokhodenko, Electrochem. Commun. 7 (2005) 477–482.
[46] S. Pang, G. Li, Z. Zhang, Macromol. Rapid Commun. 26 (2005) 1262–1265.
[47] A.V. Murugan, Electrochim. Acta 50 (2005) 4627–4636.
[48] A.V. Murugan, C.S. Gopinath, K. Vijayamohanan, Electrochem. Commun. 7 (2005) 213–218.
[49] A.V. Murugan, M. Quintin, M.-H. Delville, G. Campet, K. Vijayamohanan, J. Mater. Chem. 15 (2005) 902–909.
[50] O.Yu. Posudievsky, V.D. Pokhodenko, Russ. Chem. Bull. Int. Ed. 54 (2005) 654–659.
[51] A.V. Murugan, M. Quintin, M.-H. Delville, G. Campet, C.S. Gopinath, K. Vijayamohanan, J. Power Sources 156 (2006) 615–619.
[52] R. Bissessur, W. White, Mater Chem. Phys. 99 (2006) 214–219.
[53] A.V. Murugan, J. Power Sources 159 (2006) 312–318.
[54] S. De, A. Dey, S.K. De, Solid State Commun. 137 (2006) 662–667.
[55] G. Yang, W. Hou, X. Feng, L. Xu, Yu. Liu, G. Wang, W. Ding, Adv. Func. Mater. 17 (2007) 401–412.

[56] M.G. Kanatzidis, C.-G. Wu, H.O. Marcy, C.R. Kannewurf, J. Am. Chem. Soc. 111 (1989) 4139–4141.
[57] M.G. Kanatzidis, C.-G. Wu, H.O. Marcy, D.C. DeGroot, C.R. Kannewurf, Chem. Mater. 2 (1990) 222–224.
[58] Y.-J. Liu, D.C. DeGroot, J.L. Schindler, C.R. Kannewurf, M.G. Kanatzidis, Chem. Mater. 3 (1991) 992–994.
[59] C.O. Oriakhi, J. Chem. Educ. 77 (2000) 1138–1146.
[60] I. Capek, Nanocomposite Structures and Dispersions, Elsevier, Amsterdam, 2006.
[61] G. Kickelbick (Ed.), Hybrid Materials, Wiley-VCH, Weinheim, 2007.
[62] P.M. Ajayan, L.S. Schadler, P.V. Braun, Nanocomposite Science and Technology, Wiley-VCH, Weinheim, 2003.
[63] M. Ogawa, T. Handa, K. Kuroda, C. Kato, Chem. Lett. 19 (1990) 71–74.
[64] M. Ogawa, H. Shirai, K. Kuroda, C. Kato, Clin. Biochem. 40 (1992) 485–490.
[65] S. Yoshimoto, F. Ohashi, Ya. Ohnishi, T. Nonami, Synth. Met. 145 (2004) 265–270.
[66] S. Yoshimotoa, F. Ohashi, T. Kameyama, Solid State Commun. 136 (2005) 251–256.
[67] S. Yoshimoto, F. Ohashi, T. Kameyama, J. Polym. Sci. B: Polym. Phys. 19 (2005) 2705–2714.
[68] S. Yoshimoto, F. Ohashi, T. Kameyama, Macromol. Rapid Commun. 26 (2005) 461–466.
[69] S. Yoshimoto, F. Ohashi, T. Kameyama, Macromol. Rapid Commun. 25 (2004) 1687–1691.
[70] P. Balaž, Mechanochemistry in Nanoscience and Minerals Engineering, Springer, Berlin, 2008.
[71] Z.V. Todres, Organic Mechanochemistry and its Practical Applications, Taylor & Francis Group, Boca Raton, 2006.
[72] V.N. Muzgin, L.B. Khamzina, V.L. Zolotavin, I.Ya. Bezrukov, Analytical Chemistry of Vanadium, Nauka, Moscow, 1981 (in Russian).
[73] M. Orazem, B. Tribollet, Electrochemical Impedance Spectroscopy, Wiley-VCH, New Jersey, 2008.
[74] J.R. Macdonald, in: E. Barsoukov (Ed.), Impedance Spectroscopy Theory, Experiment, and Applications, 2nd edition, Wiley-VCH, New Jersey, 2005.
[75] O.Yu. Posudievsky, O.A. Goncharuk, V.D. Pokhodenko, Synth. Met. 160 (2010) 47–51.
[76] O.Yu. Posudievsky, O.A. Goncharuk, R. Barillé, V.D. Pokhodenko, Synth. Met. 160 (2010) 462–467.
[77] T.A. Skotheim, J.R. Reynolds (Eds.), Handbook of Conducting Polymers, 3rd edition, CRC Press, New York, 2007.
[78] O.Yu. Posudievsky, Ya.I. Kurys, S.A. Biskulova, Yu.K. Malinovsky, V.D. Pokhodenko, Theor. Exp. Chem. 38 (2002) 278–282.
[79] O.Yu. Posudievsky, G.M. Telbiz, V.K. Rossokhaty, J. Mater. Chem. 16 (2006) 2485–2489.
[80] C.-W. Kwon, A.V. Murugan, G. Campet, Active Passive Elec. Comp. 26 (2003) 171–183.
[81] J. Harreld, H.P. Wong, B.C. Dave, B. Dunn, L.F. Nazar, J. Non-Cryst. Solids 225 (1998) 319–324.
[82] I.G. Austin, N.F. Mott, Science 168 (1970) 71–77.
[83] D. Imamura, M. Miyayama, Solid State Ionics 161 (2003) 173–180.
[84] J. Scarminio, P.R. Catarini, A. Urbano, R.V. Gelamo, F.P. Rouxinol, M.A. Bica de Moraes, J. Braz. Chem. Soc. 19 (2008) 788–794.
[85] F. Huguenin, R.M. Torresi, J. Phys. Chem. C 112 (2008) 2202–2209.
[86] M.D. Levi, H. Gizbar, E. Lancry, Y. Gofer, E. Levi, D. Aurbach, J. Electroanal. Chem. 569 (2004) 211–223.